isvr Institute of Sound and Vibration Research

# An Investigation into Rail Corrugation due to Micro-Slip under Multiple Wheel/Rail Interactions

**T.X. Wu and D.J. Thompson**

ISVR Technical Memorandum No 887

April 2002

University of Southampton

# SCIENTIFIC PUBLICATIONS BY THE ISVR

***Technical Reports*** are published to promote timely dissemination of research results by ISVR personnel. This medium permits more detailed presentation than is usually acceptable for scientific journals. Responsibility for both the content and any opinions expressed rests entirely with the author(s).

***Technical Memoranda*** are produced to enable the early or preliminary release of information by ISVR personnel where such release is deemed to the appropriate. Information contained in these memoranda may be incomplete, or form part of a continuing programme; this should be borne in mind when using or quoting from these documents.

***Contract Reports*** are produced to record the results of scientific work carried out for sponsors, under contract. The ISVR treats these reports as confidential to sponsors and does not make them available for general circulation. Individual sponsors may, however, authorize subsequent release of the material.

UNIVERSITY OF SOUTHAMPTON

INSTITUTE OF SOUND AND VIBRATION RESEARCH

DYNAMICS GROUP

# An Investigation into Rail Corrugation due to Micro-Slip under Multiple Wheel/Rail Interactions

by

**T.X. Wu and D.J. Thompson**

ISVR Technical Memorandum No: 887

April 2002

Authorised for issue by
Dr M.J. Brennan
Group Chairman

ABSTRACT

The formation of short pitch corrugation on the railhead is studied by using an approach combining wheel/track dynamics, contact mechanics and wear. Multiple wheel/rail interactions are taken into account in the wheel/track dynamics. A quasi-static method based on a two-dimensional contact model is used to solve the unsteady rolling contact problem where the normal contact force and the surface curvature vary. The longitudinal slip, due to traction is considered. Corrugation growth rate is calculated at different wavelengths and at two train speeds using parameters from a British Class 87 electric locomotive and typical track. It has been found that the corrugation growth rate becomes largest when the phase of the dynamic contact force is such that its peak occurs about 135° after the corresponding trough in the roughness, i.e. just before the peak of the roughness. The growth rate is proportional to the amplitude of the dynamic contact force and is heavier at shorter wavelengths. In addition corrugation is shown to develop more quickly on track that uses stiffer pads.

CONTENTS

# 1. INTRODUCTION

Dynamic interaction between the wheel and rail occurs when a train runs on a track. Interaction forces are induced by the initial irregularities that are present on the wheel and rail contact surfaces, for example roughness. These varying contact forces cause uneven wear on the railhead. After the passage of millions of wheelsets, the irregularities on the railhead become larger and larger at some wavelengths, whereas at others they are unaffected or even suppressed. These wear patterns can form into corrugation, a more or less periodic irregularity on the running surface of the rail.

Corrugation is an unwelcome phenomenon because it causes increased dynamic interaction forces between the wheel and rail and thus vibration, noise and damage problems. Grassie and Kalousek [1] classified rail corrugations into six types by their characteristics and mechanisms. Amongst them, in terms of railway rolling noise impact, short pitch or roaring rail corrugations, whose wavelength is about 25-80 mm, are of greatest concern to the railway industry. They give rise to excitation predominantly in the frequency range 50-1500 Hz and cause severe track damage and noise. Observations made in the field indicate that the damage mechanism for short pitch corrugations is wear and their wavelength varies little with the predominant speed of trains [2]. Many attempts to explain the corrugation process have been made, but no fully satisfactory explanation is yet available for the wavelength fixing mechanism of short pitch corrugation.

It is recognised that short pitch corrugation on the running surface of the rail is formed by a process of periodic wear during the rolling passage of the wheels. Many studies are based on the hypothesis that short pitch corrugation arises from a combination of the wheel/rail dynamics, rolling contact mechanics and wear. A common feature of this hypothesis is that an initially random railhead roughness gives rise to variations in the normal contact force between the wheel and rail and consequently to variations of slip and wear in the contact patch. To make corrugation growth possible at some wavelengths, it was believed that the phase should be such that the contact force between the wheel and rail reaches its maximum near the crest of a corrugation and has a minimum around the troughs. This is because a smaller contact force results in a larger slip zone in the contact area and thus more frictional work and wear according to the rolling contact theory of elastic bodies [3, 4].

Grassie and Johnson [5] calculated the frictional energy dissipation in the slip zone of the contact patch as a wheel rolls over a sinusoidally corrugated rail. No adequate mechanism explaining the cause of corrugation was found because there was no maximum in the energy

dissipation at a particular fixed wavelength independent of vehicle speed. Moreover the dissipation for typical speeds and wavelengths was not a maximum in the troughs of an existing corrugation. Frederick [6] developed a method of phase relation analysis between the wheel/rail normal contact force, lateral and longitudinal forces, creep and wear based on a linear analysis of small perturbations. This was used to investigate the corrugation growth rate at different frequencies, defined by the wavelength of corrugation and the wheelset speed. Hempelmann et al. [7] predicted the formation of short pitch corrugation using a similar linear model combining transient dynamics of a single wheel/rail interaction and a wear feedback loop. It was shown that the railhead corrugation is associated with the pinned-pinned mode of the track at about 1 kHz and its wavelength is related to this frequency and a particular vehicle speed.

Similar studies based on the wheel/rail dynamics in the time-domain have been carried out by Igeland [8], Igeland and Ilias [9] and Nielsen [10]. In [8] a bogie/track interaction model (i.e. including two wheels) was used for wheel/rail dynamics and the simulations showed that the spectral density of the railhead wear depended on frequency (wavelength) almost in the same way as the normal contact force. This feature resulted from the assumption that the frictional power is proportional to the normal contact force although the relation between them is actually non-linear. Wear was calculated in [8-10] in such a way that it was assumed to occur only at a single point for each time interval rather than to be distributed in a slip zone of the contact patch, although an improvement was considered in [9] by shifting the wear centre towards the trailing edge of the contact patch.

Other proposed hypotheses of rail corrugation are associated with spin creep [11], the development by wear of close conformity and roll-slip oscillation between the wheel and rail [2]. However, spin creep has been ruled out by experimental investigation [12]. Also Bhaskar's work was intended to demonstrate the roll-slip phenomenon but did not produce a satisfactory explanation [13, 14].

An interesting study of rail corrugation has been carried out by Nielsen [15]. In [15] a non-linear wear model was developed for the contact between a cylinder rolling over a periodically varying surface. In this model the wheel/rail dynamics was totally neglected and the normal contact force was assumed to be constant. The only factor causing corrugation in the model was the wheel and rail surface geometry. Wear was calculated in the slip zone of the contact patch. Using this model the critical wavelengths at which corrugation growth occurs have been predicted.

In order to get a better understanding of the formation of short pitch corrugation, some significant practical factors have to be take into account in a calculation model, which should combine the wheel/track dynamics, contact mechanics and wear. For example, the usual model of a single wheel on a rail neglects the fact that multiple wheel/rail interactions occur when a train passes over the track. It has been found, in a recent study of noise generation, that the spectrum of the wheel/rail contact force may have several peaks at different frequencies due to the wave reflections between the wheels on a rail [16]. For the interaction between a whole train and the track, the wavelengths of short pitch corrugation can therefore be expected to be associated with several frequencies rather than only one frequency. The corresponding behaviour of the normal contact forces under multiple wheel/track interactions has been studied by Wu and Thompson [17].

In addition the wheel/rail contact patch may be divided into stick and slip zones and wear occurs only in the slip zone. Moreover, wear is an accumulation process as the slip zone continuously moves forward during rolling of the wheel over the track, with the contact patch dimension varying with changes in the normal contact force and contact geometry. If these factors are taken into account, the phase conditions of the contact force under which corrugation growth occurs might not be as simple as described above.

In this report the mechanism of short pitch corrugation is studied by combining wheel/track dynamics, contact mechanics and wear. The practical factors affecting corrugation, stated above, are taken into account in the model. Firstly, the concepts of multiple wheel/rail dynamics are introduced and the features of the normal contact force under multiple wheel/rail interactions are reviewed. The wheel/rail rolling contact is represented by a disc and a sinusoidal surface respectively giving a two-dimensional contact model. Then, an approach is developed to calculate wear on the railhead due to unsteady rolling contact, where the normal contact force and the surface curvature vary with time under the action of a steady longitudinal traction. A quasi-static method is used to determine the length of the contact patch and the boundary between the stick and slip zones in each small time interval. Longitudinal frictional work and wear are calculated throughout the slip zone and accumulated to form a new profile of the railhead after a wheel passage. Finally, combining the features of multiple wheel/rail interactions, unsteady rolling contact and the detailed wear calculations, corrugation growth is predicted at different frequencies or wavelengths for typical train speeds.

## 2. NORMAL CONTACT FORCE OF MULTIPLE WHEEL/RAIL INTERACTIONS

### 2.1. Multiple wheel/rail interactions

In practice a train consists of multiple wheels on each rail and multiple wheel/rail interactions occur. Figure 1 shows a track interacting with four wheels. These wheels represent a pair of bogies of an electric locomotive. Consider first a roughness excitation at wheel 1 and no excitations at wheels 2, 3 and 4. The interaction force at wheel 1 caused by the roughness excitation generates an incident wave propagating along the rail and the incident wave interacts with wheels 2, 3 and 4. This leads to the generation of 'passive' interaction forces $P_{21}$, $P_{31}$ and $P_{41}$ between the wheel and rail at each contact position [16]. Here the subscripts $ji$ indicate that $P_{ji}$ is at position $j$ and caused by the roughness at $i$. The passive interaction forces also generate waves propagating in both directions from the respective contact points. The generated waves in the negative direction then travel back to wheel 1 and interact again with it. The interaction force at wheel 1 therefore results from the roughness at wheel 1 and from the reflected waves from wheels 2, 3 and 4. This is much different from a single wheel/rail interaction where no waves are reflected from other wheels.

When the roughness excitation is considered to be only at wheel 1 and no excitations at other wheels, the interaction force at wheel 1, $F_1$, is called the 'active' interaction force. On the other hand, when the interaction force at wheel 1 is considered to be caused by roughness excitations at other wheels and with no roughness being at wheel 1, the interaction force at wheel 1 is called a 'passive' interaction force, for example, $P_{12}$, $P_{13}$ and $P_{14}$. In general, roughness exists at each wheel/rail contact position and thus the wheel/rail interaction force is a combination of both active and passive forces. For a linear system the total interaction force is the sum of the active and passive forces, due to superposition [16].

### 2.2. Active interaction force

The features of the forces for multiple wheel/rail interactions have been studied in [17]. The active contact force $F_i$ at each wheel can be calculated using a relative displacement (roughness) excitation model proposed in [17]:

$$F_i(\omega) = -\frac{r(\omega)}{\alpha^W(\omega) + \alpha^C(\omega) + \alpha_i^R(\omega)}, \tag{1}$$

where $r$ is the relative displacement amplitude (roughness) between the wheel and rail, $\alpha^W$, $\alpha^C$ and $\alpha_i^R$ are the point receptances (displacement divided by force) of the wheel, contact spring and rail respectively and $\omega$ is the circular frequency of the excitation. The rail receptance is

calculated using a track model in which multiple wheels are present on the rail. All variables in equation (1) are complex and the common term $e^{i\omega t}$ is omitted.

Figures 2 and 3 show the active normal contact forces at wheels 1 and 2, with four wheels interacting with the track, as shown in Figure 1. The interaction forces are calculated due to 1 μm roughness excitation at each frequency using the model and method developed in [17]. The distances between wheels are shown in Figure 1 and correspond to a Class 87 electric locomotive which has four driving wheelsets, with the wheel mass being 1350 kg each. The sleeper span of the track is 0.6 m and the railpad stiffness is 70 kN/mm. In Figure 2 wheel 1 is chosen to be at a sleeper and thus wheel 2 is at mid-span. In Figure 3 wheel 1 is at mid-span and wheel 2 is at a sleeper. For comparison, the contact forces of a single wheel/rail interaction are also shown in Figure 2.

From Figures 2 and 3 the contact forces under multiple wheel/rail interactions can be seen to be greatly different from the single wheel/rail interaction and mostly have larger amplitudes. The contact forces show many peaks in the frequency region 600-1000 Hz due to the wave reflections from the adjacent wheels. Compared with wheel 1, the contact force at wheel 2 shows more peaks because wheel 2 receives wave reflections from both sides. In the single wheel/rail interaction there is only one peak in the contact force at about 1080 Hz, which is just above the pinned-pinned resonance at 1050 Hz, when the wheel is at mid-span. Below 1 kHz there are no big differences between the two cases of wheel 1 at mid-span and at a sleeper, nor between the corresponding results for wheel 2. When multiple wheel/rail interactions are taken account of, it may be expected that short pitch corrugation is associated with multiple frequencies at which peaks occur in the normal contact forces, rather than with only one frequency as found for a single wheel /rail interaction.

### 2.3. Passive interaction force

The effects on short pitch corrugation of passive interaction forces caused by the roughness at other wheels can be ignored. This is because the minimal distance between two wheels is at least many tens of wavelengths of the railhead irregularities considered. As the irregularities are not perfectly sinusoidal, the phase of the passive contact force can be assumed to vary randomly relative to that of the active force, and these forces may be assumed to be uncorrelated. As a result the passive wheel/rail interaction forces will generally have no contribution to the growth of short pitch corrugation, since sometimes they have the effects of enhancing the troughs and sometimes they have the effects of removing material from the crests. The passive interaction forces are therefore not considered further here.

## 3. CALCULATIONS OF MICRO-SLIP AND WEAR

As in [5], the contact mechanics of the wheel/rail system are simplified to a two-dimensional (plane strain) problem, i.e. a cylindrical wheel of radius $R_w$ (575 mm) rolling at constant speed $V$ over a sinusoidally corrugated rail, as shown in Figure 4. The original corrugation on the railhead is of wavelength $\lambda$ and given as

$$r(l) = \Delta \sin \frac{2\pi}{\lambda} l , \tag{2}$$

where $\Delta$ is the small amplitude of the corrugation and $l = Vt$ is the rolling distance. Note that $r$ is positive downwards and $V$ is negative as shown in Figure 4. The curvature of the corrugation can be derived from (2) and is given as

$$\frac{1}{R_r} \approx \frac{d^2 r}{dl^2} = -\left(\frac{2\pi}{\lambda}\right)^2 \Delta \sin \frac{2\pi}{\lambda} l . \tag{3}$$

The normal contact force $F$ between the wheel and rail varies at a circular frequency $\omega = 2\pi V/\lambda$ defined by the corrugation wavelength $\lambda$ and the wheel speed $V$. Assuming a linear model, it consists of a static component $F_s$ and a dynamic one of amplitude $F_d$,

$$F = F_s + F_d \sin\left(\frac{2\pi}{\lambda} l - \phi_d\right). \tag{4}$$

Only the active interaction force is taken into account in the dynamic component and its amplitude $F_d$ and phase $\phi_d$ relative to $r(l)$ are functions of frequency as shown in Figures 2 and 3 in the last section.

### 3.1. Unsteady wheel/rail rolling contact

Since the normal contact force and the contact geometry are functions of time (or distance), the rolling contact becomes unsteady. A quasi-static method is used to solve this unsteady rolling contact problem. It is assumed that in each tiny interval of time the contact mechanics is in a steady state apart from the longitudinal slip velocity. The unsteady term caused by the varying contact force and geometry is taken into account in the slip velocity because it is crucial to the frictional work and wear, hence the cause of corrugation.

It is assumed that the wheel and rail deform as elastic half-spaces and thus Hertz theory holds. To be similar to the steady rolling contact, it is assumed that the contact patch in each time interval can be divided into a stick zone in the leading area and a slip zone in the trailing area. According to Carter [18], as also used by [5] and [15], the longitudinal traction distribution is described as in Figure 5, where the origin of coordinates is fixed in the middle

of the contact patch and moves with the wheel at speed $V$. In the slip zone the traction $q(x, l)$ is determined by

$$q(x,l) = \mu p(x,l), \tag{5}$$

where $\mu$ is the friction coefficient and $p(x, l)$ is the normal pressure and can be calculated using

$$p(x,l) = \frac{F(l)}{\pi a(l) b}\left\{1-\left(\frac{x}{a(l)}\right)^2\right\}^{1/2}, \tag{6}$$

where $F(l)$ is the normal contact force defined by equation (4), $b$ is half the wheel width (in contact) and $a(l)$ is half the contact patch length and given as

$$a(l) = \left\{\frac{4F(l)R(l)}{\pi b E'}\right\}^{1/2}. \tag{7}$$

In equation (7) $E'$ is the equivalent modulus,

$$E' = \frac{E}{1-\nu^2}, \tag{8}$$

where $E$ is the Young's modulus and $\nu$ is the Poisson's ratio. $R(l)$ is the equivalent radius of wheel/rail contact and is determined by

$$\frac{1}{R(l)} = \frac{1}{R_w} + \frac{1}{R_r(l)}, \tag{9}$$

where $1/R_w$ is the wheel curvature and $1/R_r(l)$ is the rail curvature at position $l$.

The slip velocity $v(x, l)$ for unsteady rolling contact without spin is given as, [5],

$$v(x,l) = V\left\{\xi + \frac{\partial u(x,l)}{\partial x} + \frac{\partial u(x,l)}{\partial l}\right\}, \tag{10}$$

where $\xi$ is the longitudinal creep and $u(x, l)$ is the relative displacement in the longitudinal direction between the wheel and rail. For the two-dimensional (plane strain) contact problem, $\xi$ is given by, [4],

$$\xi = \frac{\mu a(l)}{R(l)}\left\{1-\left(1-\frac{Q}{\mu F(l)}\right)^{1/2}\right\}, \tag{11}$$

where $Q$ is the total longitudinal traction and results from an integration of the traction over the stick and slip zones. The relative displacement $u(x, l)$ is generally dependent upon the traction throughout the contact patch. It is very difficult to obtain an analytical relation between the traction and $u(x, l)$ for unsteady rolling. In order to calculate $u(x, l)$, an

approximation based on an elastic foundation model is used, in which $u(x, l)$ is assumed to be associated only with the local traction, such that

$$u(x,l) = -q(x,l)/\beta\,, \tag{12}$$

where $\beta$ is a tangential stiffness whose value is calculated in [5] by

$$\beta = \frac{1}{16}\left\{\frac{b}{F(l)R(l)}(\pi E')^3\right\}^{1/2}. \tag{13}$$

Substituting for $\beta$ from equation (13) and for $q(x, l)$ from equations (5), (6) and (7), $u(x, l)$ is given as

$$u(x,l) = -\frac{4\mu}{\pi(\pi bE')^{1/2}}\left\{\frac{4F^2(l)}{\pi bE'} - \frac{F(l)}{R(l)}x^2\right\}^{1/2}. \tag{14}$$

Its derivatives with respect to $x$ and $l$ are

$$\frac{\partial u}{\partial x} = \frac{4\mu}{\pi(\pi bE')^{1/2}}\left\{\frac{4F^2}{\pi bE'} - \frac{F}{R}x^2\right\}^{-1/2}\frac{F}{R}x\,, \tag{15}$$

$$\frac{\partial u}{\partial l} = \frac{4\mu}{\pi(\pi bE')^{1/2}}\left\{\frac{4F^2}{\pi bE'} - \frac{F}{R}x^2\right\}^{-1/2}\left\{\left(\frac{1}{R}\frac{dF}{dl} + F\frac{d(1/R)}{dl}\right)\frac{x^2}{2} - \frac{4F}{\pi bE'}\frac{dF}{dl}\right\}. \tag{16}$$

Using equations (10), (11), (15) and (16), the longitudinal slip velocity between the wheel and rail can be determined.

### 3.2. Wear calculation

Wear occurs only in the slip zone of the contact patch. The boundary between the stick and slip zones can be determined by

$$x_b = a - \frac{R}{\mu}\xi\,. \tag{17}$$

Calculation of wear during rolling contact is an accumulation process. In each tiny time interval wear can be calculated numerically as follows,

$$W_t(x) = Kq(x,t)v(x,t)\Delta t\,, \tag{18}$$

where $W_t(x)$ is the wear at position $x$ which is in the slip zone, $q(x, t)$ is the traction, $v(x, t)$ is the slip velocity, $\Delta t$ represents a tiny time interval and $K$ is a material-related constant. In the present study the value of $K$ is chosen to be $2.5\times10^{-9}$ kg/Nm [10]. The units of $W_t(x)$ are therefore kg/m$^2$, the mass loss per unit area. The subscript $t$ of $W_t(x)$ means that the wear is generated only in the time interval $[t, t+\Delta t]$ and at $x$ which is in the local coordinates of the contact patch. The total wear at position $l$, $W(l)$, which is in the global coordinates, is therefore an accumulation of the wear generated in each time interval $\Delta t$ during the rolling

contact. If the rolling speed of the wheel is known as $V$, and the wheel centre position in the longitudinal direction is known as $l = Vt$, then equation (18) can be rewritten as

$$W_l(x) = Kq(x,l)v(x,l)\Delta l / V \,. \tag{19}$$

Using $l$ instead of $t$ makes equation (19) consistent with the previous analysis. As a result the accumulated wear depth $\Delta r(l)$ on the railhead surface after one wheel passage is obtained by

$$\Delta r(l) = W(l) / \rho \,, \tag{20}$$

where $\rho$ is the material density of the rail, $\rho = 7800$ kg/m$^3$.

## 4. RAIL CORRUGATION GROWTH

### 4.1. The effects on wear of dynamic force and corrugation wavelength

Before calculating the growth of rail corrugation, it is helpful to explore the effects on wear of the dynamic contact force and the corrugation wavelength. Calculations are carried out for three cases of wavelength 25 mm, 40 mm and 60 mm, each with 10 μm amplitude. The static contact force is chosen to be 100 kN. The amplitude of the dynamic contact force is given two values in the calculations, 25 kN and 40 kN, which are assumed at this stage, though in practice they depend on the roughness amplitude. The total traction between the wheel and rail is assumed to be constant, $Q$ = 15 kN. The frictional coefficient $\mu$ is taken as 0.3. Under 100 kN static contact force and the given conditions, the longitudinal creep $\xi$ is around 0.1 %. To explore how the phase of the dynamic force affects wear, four phase lag values are assumed, $\phi_d$ = 45°, 90°, 135° and 180°. In the sign convention adopted, when the phase lag of the dynamic force is zero, it means that the dynamic force reaches its minimum at the crests and its maximum at the troughs of the corrugation respectively.

Wear induced after one wheel passage $\Delta r$ is shown in Figures 6-8. For comparison the shape of the original sinusoidal corrugation is also shown in the figures. Note that wear occurs along the whole rail, but that it is greater at some locations than others due to dynamic effects. Comparing the figures, it can be seen that wear is heavier at shorter wavelengths and increases as the amplitude of the dynamic contact force increases, although the relation between the contact force and wear is non-linear. It can be observed from Figures 6-8 that corrugation might not grow when the phase lag of the dynamic force is 180° or 45°, as the wear is greatest away from the troughs. Instead, the corrugation growth becomes maximal at a phase lag of about 135°. This probably results from a combination of factors: (a) wear occurs only in the slip zone, (b) wear is an accumulation process throughout the continuous rolling

over the corrugation, (c) the dynamic force and contact geometry vary with the position of the wave and so do the slip velocity and the frictional work. As wear unevenly occurs on a wave, corrugation is developed with the generation of short wavelength components.

### 4.2. Rail corrugation growth

Rail corrugation is predicted by combining the wheel/track dynamics and contact mechanics. The active wheel/rail contact force is calculated using a multiple wheel/rail interaction model developed in [17], some results of which were shown in section 2. Wear is calculated using the method introduced in section 3. Since the dynamic contact force is generated by the corrugation on the railhead, the frequency of the contact force, $f$, is associated with the corrugation wavelength, $\lambda$, and the wheel speed, $V$, by $f = V/\lambda$.

After the wear depth $\Delta r$ has been calculated using equation (20), the new profile of the rail corrugation after one wheel passage is known as

$$r_n(l) = r(l) + \Delta r(l), \tag{21}$$

where the original corrugation $r(l)$ is sinusoidal with amplitude $\Delta$ and wavelength $\lambda$ as in equation (2). In order to measure whether the original corrugation at wavelength $\lambda$ is magnified or flattened, a Fourier transform of $r_n$ is performed and the component at wavelength $\lambda$ is used to determine the corrugation growth rate which is given as

$$G(\lambda) = \frac{R_n(\lambda) - \Delta}{\Delta}, \tag{22}$$

where $R_n(\lambda)$ is the magnitude of the component at wavelength $\lambda$ of the new corrugation profile after one wheel passage. If the value of $G(\lambda)$ is positive, the original corrugation is magnified, otherwise it is flattened.

The corrugation growth is predicted for a Class 87 electric locomotive interacting with a track consisting of UIC 60 rail with three types of railpad. The pad stiffness is chosen to be 70, 300 and 1000 kN/mm, respectively, representing soft, medium and stiff pads. The wheel/rail interaction forces are calculated based on an original corrugation of 10 μm amplitude for each wavelength. The static normal contact force is assumed to be 100 kN. Two wheel speeds are used in the calculations, 120 and 180 km/h. Other parameters are consistent with the previous calculations in this report. Calculations are carried out for the dynamic contact force at each frequency, which corresponds to the wavelengths associated with the speeds. Results are shown in Figures 8-13 in terms of the amplitude and phase of the active contact forces for wheels 1 and 2 at four different positions in a sleeper span and the corrugation growth rate, as defined by equation (22).

Figures 8 and 9 are the results from the soft rail pad. The dynamic contact force can be seen to have many peaks in the frequency region 500-1200 Hz due to the wave reflections between the wheels. The highest peaks occur just above the pinned-pinned resonance frequency when the wheels are between two sleepers. This is because the rail receptance there is out of phase with the receptance of the contact stiffness but their amplitudes are equal. It occurs even though the pinned-pinned resonance peak in the rail receptance may be suppressed due to the wave reflections from other wheels, as discussed in [16]. As a result, the wheel/rail interaction force reaches a peak according to equation (1). As demonstrated in section 4.1, corrugation grows if the dynamic contact force is large and its phase lag is around 135°. It can be seen from Figures 8 and 9 that the corrugation growth rate shows three peaks for wheel 1 and five peaks for wheel 2 in the frequency region 600-1200 Hz. This range corresponds to wavelengths 28-56 mm at a speed of 120 km/h or 42-83 mm at 180 km/h. These peaks are associated with the peaks in the dynamic contact force with a phase lag near 135°. The force peaks under 600 Hz do not cause a high corrugation rate because the phase lag there is only about 90°. The corrugation growth rate is generally higher at a speed of 120 km/h, compared to that at 180 km/h. This is because the wavelength is shorter at 120 km/h than at 180 km/h for the same frequency, and wear is larger at the shorter wavelengths as shown in Figures 5-7.

Figures 10 and 11 are the results from the medium pad and Figures 12 and 13 are those from the stiff pad. The peaks in the dynamic contact force for the medium pad case are not very high for frequencies below 1 kHz because the wave propagation in the rail decays quickly due to the higher damping of the medium pad. For the stiff pad case, there are no peaks in the contact force below 1 kHz and the contact forces are the same for both wheel 1 and wheel 2. This indicates that, due to the high damping of the track caused by the stiff pad, the dynamic behaviour of multiple wheel/rail interactions are the same as for a single wheel/rail interaction. However, the peaks near the pinned-pinned resonance are very high due to use of the medium and stiff pads. These peaks in the contact force cause high rates in the corrugation growth at wavelength around 25-30 mm at 120 km/h or 38-45 mm at 180 km/h. Thus the use of the stiffer pad results in a quicker formation of short pitch corrugation.

## 5. CONCLUSIONS

The formation of short pitch corrugation is studied by using an approach combining wheel/track dynamics, contact mechanics and wear. Multiple wheel/rail interactions are taken into account in the wheel/track dynamics. The active wheel/rail contact forces are assumed to be responsible for the rail corrugation. In the contact mechanics a quasi-static method is used to determine the contact patch and the boundary between the stick and slip zones due to unsteady rolling contact where the normal contact force and the surface curvature vary. The total wear on the railhead is calculated by accumulating the wear in the slip zone in each time step as the wheel rolls over the track. The corrugation growth rate is calculated at different wavelengths and at two train speeds using parameters corresponding to a Class 87 electric locomotive and UIC 60 rail with three pad stiffnesses.

The dynamic contact force under multiple wheel/rail interactions has many peaks at different frequencies due to the wave reflections between the wheels when using softer rail pads. It is therefore expected that the wavelengths of short pitch corrugation are associated with several frequencies rather than only one frequency as in the case of a single wheel/rail interaction. Since the normal contact force and the contact geometry are functions of time or distance, the rolling contact becomes unsteady, so that the contact patch, the boundary of the stick and slip zones and the slip velocity between the wheel and rail also vary with time or distance. In addition, wear only occurs in the slip zone and corrugation results from an accumulation process of wear. As a result of a combination of all these factors, it has been found that the corrugation growth rate becomes largest when the phase of the dynamic contact force is such that its peak occurs about 135° after the corresponding trough in the roughness, i.e. just before the peak of the roughness. It is also found that wear is heavier at shorter wavelengths and increases with the amplitude of the dynamic contact force. In addition corrugation develops more quickly using stiffer pads than using softer pads, although the medium pad considered has the largest growth rate for a wheel at midspan.

Some errors are induced in the calculations of the slip velocity and thus the frictional work and wear by using the elastic foundation model. In addition components of short wavelengths in corrugation generated after each wheel passage are not considered in the calculations of the growth rate. It is anticipated that the first deficiency will not cause problems, because wear at each point of a roughness wave experiences the same calculations and the formation of corrugation is based on a comparison of different positions. A model in the time-domain may be needed to overcome the second deficiency. It is beyond the scope of this report.

## REFERENCES


1. S. L. Grassie and J. Kalousek, Rail corrugation: characteristics, causes and treatments. *Proc. Instn Mech. Engrs,* Part F, 207 (1993) 57-68.
2. J. Kalousek and K. L. Johnson, An investigation of short pitch wheel and rail corrugation on the Vancouver mass transit system. *Proc. Instn Mech. Engrs,* Part F, 206 (1992) 127-135.
3. J. J. Kalker, Three-dimensional elastic bodies in rolling contact. Kluwer Academic Publishers, Dordrecht, 1990.
4. K. L. Johnson, Contact mechanics. Cambridge University Press, Cambridge, 1985.
5. S. L. Grassie, and K. L. Johnson, periodic microslip between a rolling wheel and a corrugated rail. *Wear,* 101 (1985) 291-309.
6. C. O. Frederick, A rail corrugation theory. *Proc. Int. Symp. on Contact Mechanics and Wear of Wheel/Rail Systems II,* Kingston, Rhode Island, July 1986, University of Warterloo Press, 1987, 181-211.
7. K. Hempelmann, F. Hiss, K. Knothe and B. Ripke, The formation of wear patterns on rail tread. *Wear,* 144 (1991) 179-195.
8. A. Igeland, Railhead corrugation growth explained by dynamic interaction between track and bogie wheelsets. *Proc. Instn Mech. Engrs,* Part F, 210 (1996) 11-20.
9. A. Igeland and H. Ilias, Rail head corrugation growth predictions based on non-linear high frequency vehicle/track interaction. *Wear,* 213 (1997) 90-97.
10. J. C. O. Nielson, Numerical prediction of rail roughness growth on tangent tracks. *Proceedings of the 7th International Workshop on Railway Noise*, Portland, Maine, October 2001.
11. D. E. Newland, On the time-dependent spin creep of a railway wheel. *J. Mech. Engng Sci.,* 24 (1982) 55-64.
12. S. L. Grassie, An investigation into the generation of corrugation by transient spin creep. *Wear,* 101 (1985) 161-174.
13. A. Bhaskar, K. L. Johnson, G. D. Wood and J. Woodhouse, Wheel-rail dynamics with closely conformal contact Part 1: dynamic modelling and stability analysis. *Proc. Instn Mech. Engrs,* Part F, 211 (1997) 11-26.
14. A. Bhaskar, K. L. Johnson, G. D. Wood and J. Woodhouse, Wheel-rail dynamics with closely conformal contact Part 2: forced response, results and conclusions. *Proc. Instn Mech. Engrs,* Part F, 211 (1997) 27-40.

15. J. B. Nielsen, Evolution of rail corrugation predicted with a non-linear wear model. *Journal of Sound and Vibration,* 227 (1999) 915-933.
16. T. X. Wu and D. J. Thompson, Vibration analysis of railway track with multiple wheels on the rail. *Journal of Sound and Vibration,* 239 (2001) 69-97.
17. T. X. Wu and D. J. Thompson, Behaviour of the normal contact force under multiple wheel/rail interaction. *Vehicle System Dynamics* (in press).
18. F. W. Carter, On the action of a locomotive driving wheel. *Proceedings of the Royal Society of London,* A112 (1926) 151-157.

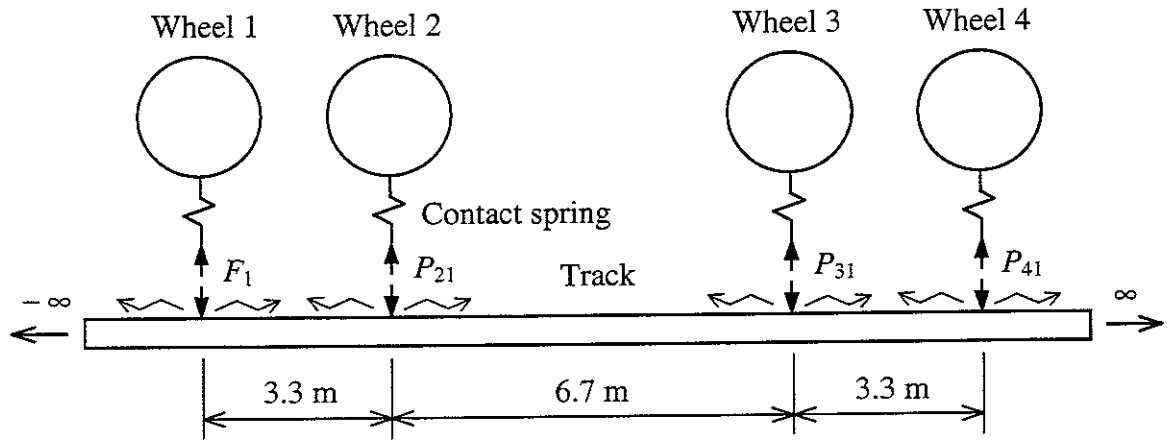


Figure 1. Multiple wheel/track interactions. Wheel 1 is 'active' with roughness excitation. Other wheels are 'passive' without roughness excitations.

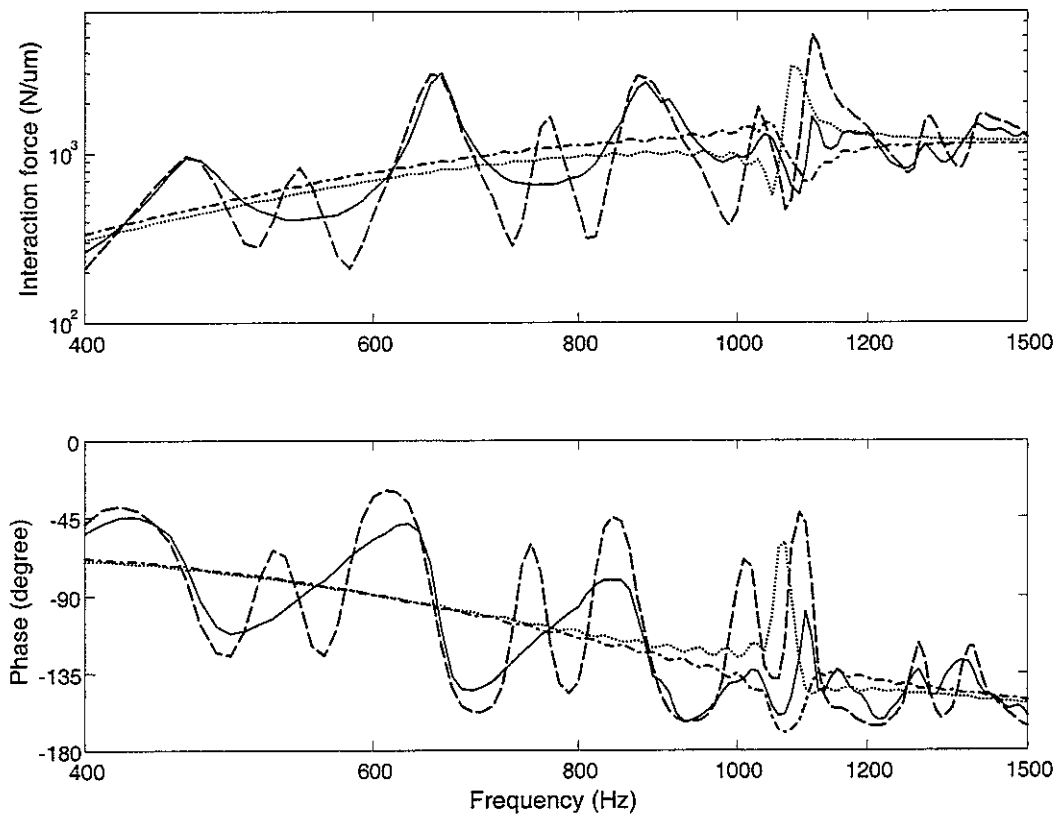


Figure 2. Active interaction forces with four wheels on the rail. Position I: — wheel 1 (at sleeper), ---- wheel 2 (at mid-span), -·-·- single wheel/rail interaction (at sleeper), ····· single wheel/rail interaction (at mid-span).

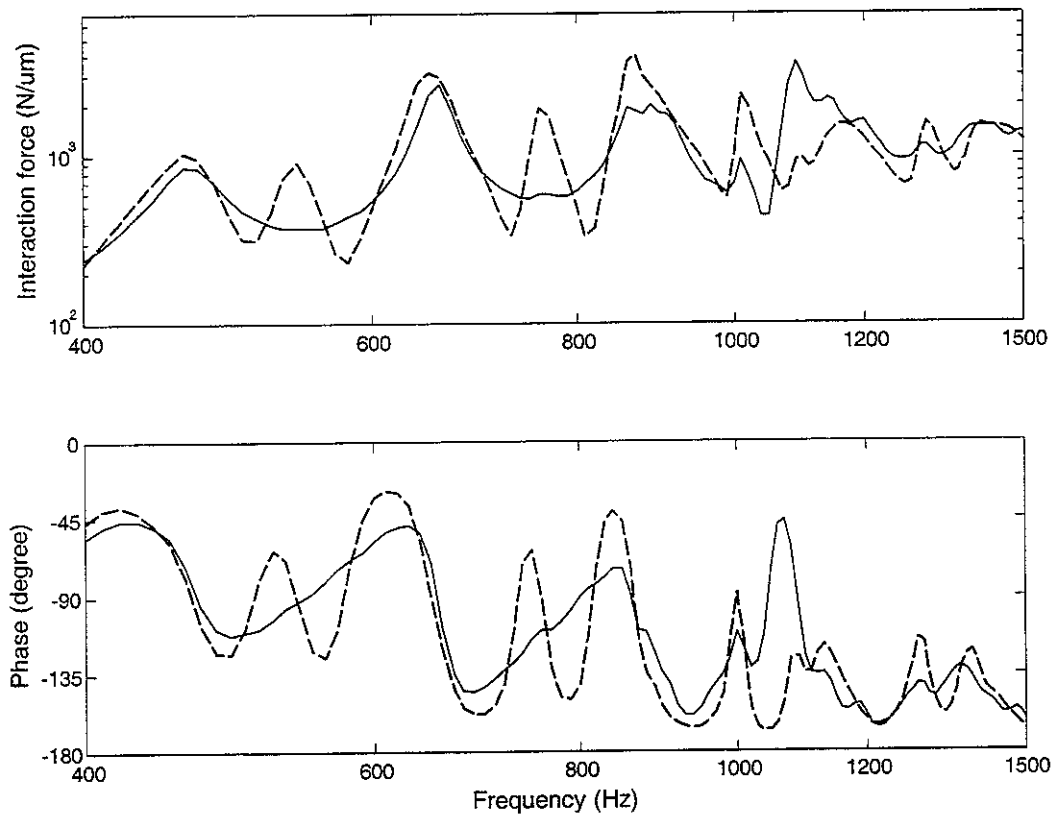


Figure 3. Active interaction forces with four wheels on the rail. Position II: — wheel 1 (at mid-span), ---- wheel 2 (at sleeper).

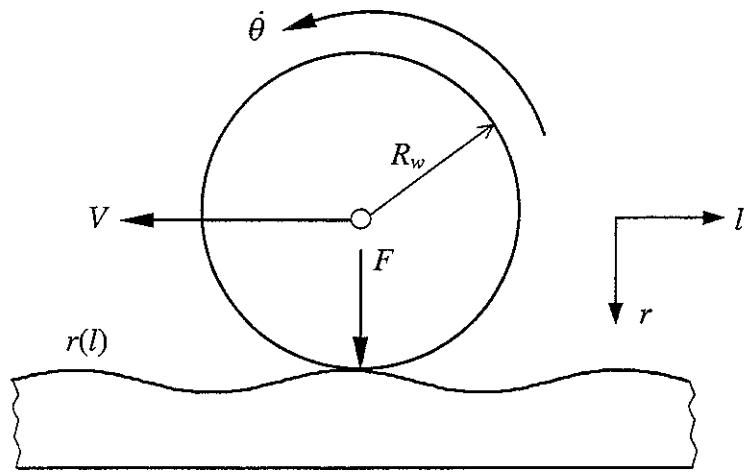


Figure 4. A wheel rolling over a sinusoidal corrugation $r(l)$. $V$ as shown is negative.

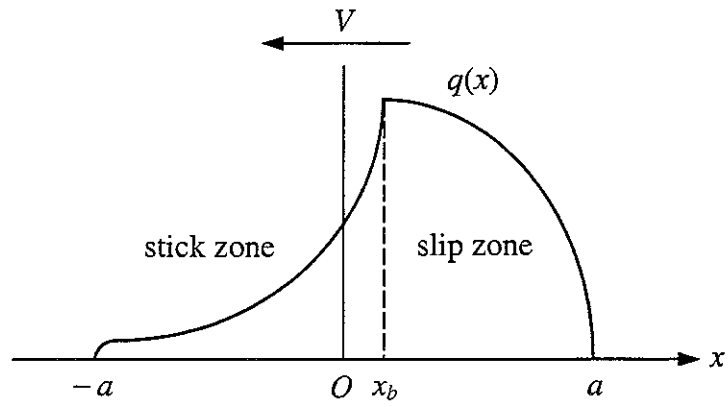


Figure 5. Assumed longitudinal traction distribution. $a$ is half the contact patch length and $x_b$ is the boundary of the stick and slip zones.

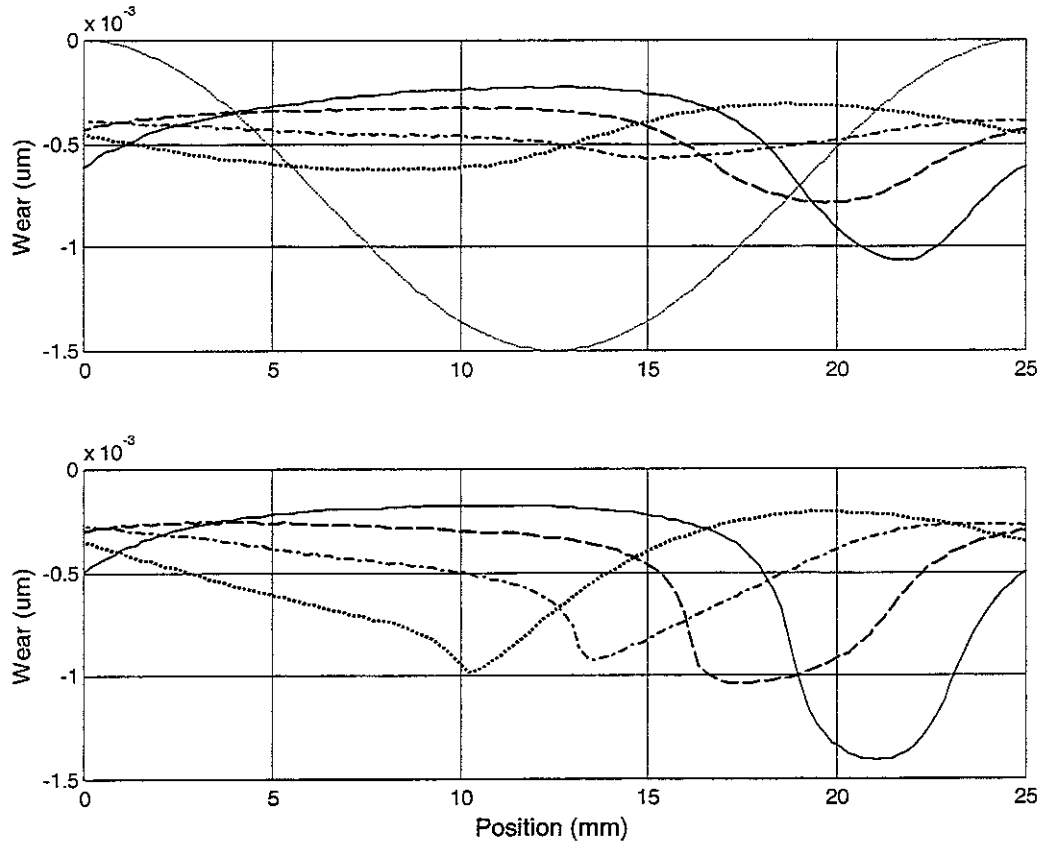


Figure 6. Wear due to micro-slip. Static contact force $F_s$ = 100 kN, magnitude of dynamic force $F_d = 0.25F_s$ for the top Figure and $F_d = 0.4F_s$ for the bottom one, frictional coefficient $\mu$ = 0.3, total traction $Q$ = 15 kN, wheel radius $R_w$ = 575 mm, half contact patch width $b$ = 8 mm, corrugation wavelength $\lambda$ = 25 mm, amplitude $\Delta$ = 10 μm. — for dynamic force phase lag $\phi_d = 45°$, ---- $\phi_d = 90°$, ----- $\phi_d = 135°$, ····· $\phi_d = 180°$, ····· (light) original corrugation of one wavelength (not to scale, shown to indicate the phase relative to the wear).

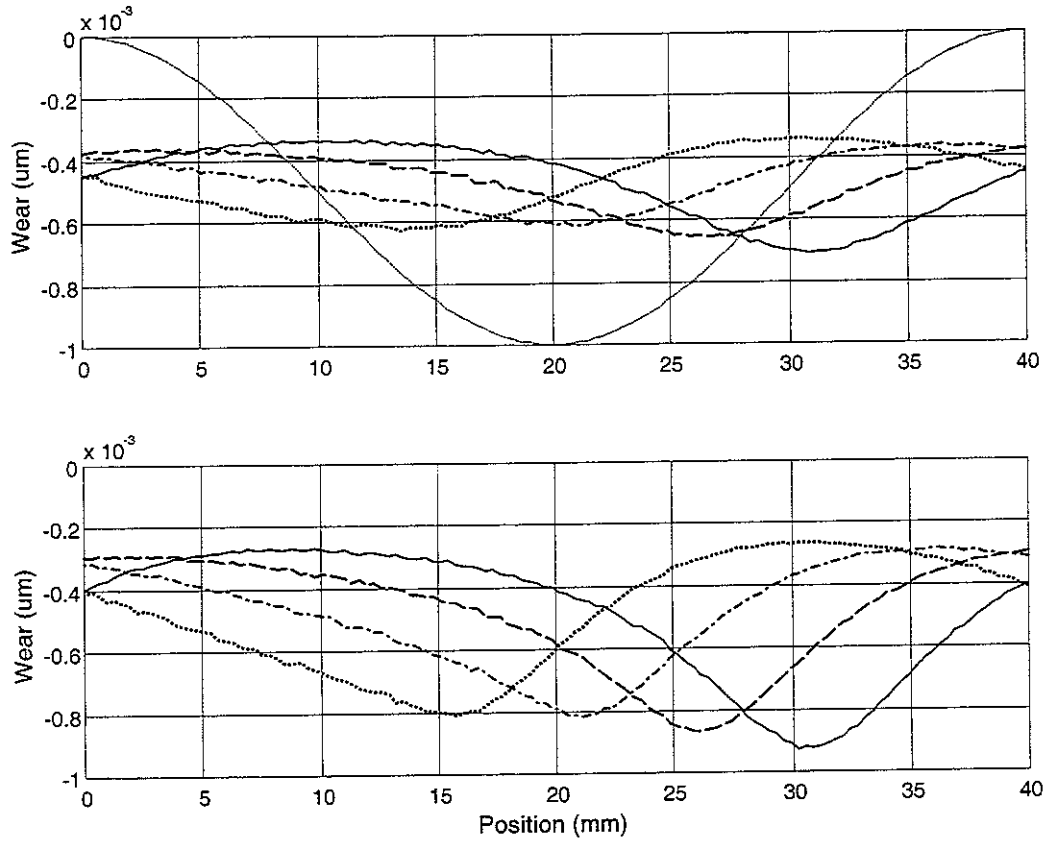


Figure 7. Wear due to micro-slip for corrugation wavelength $\lambda = 40$ mm, key as for Figure 6.

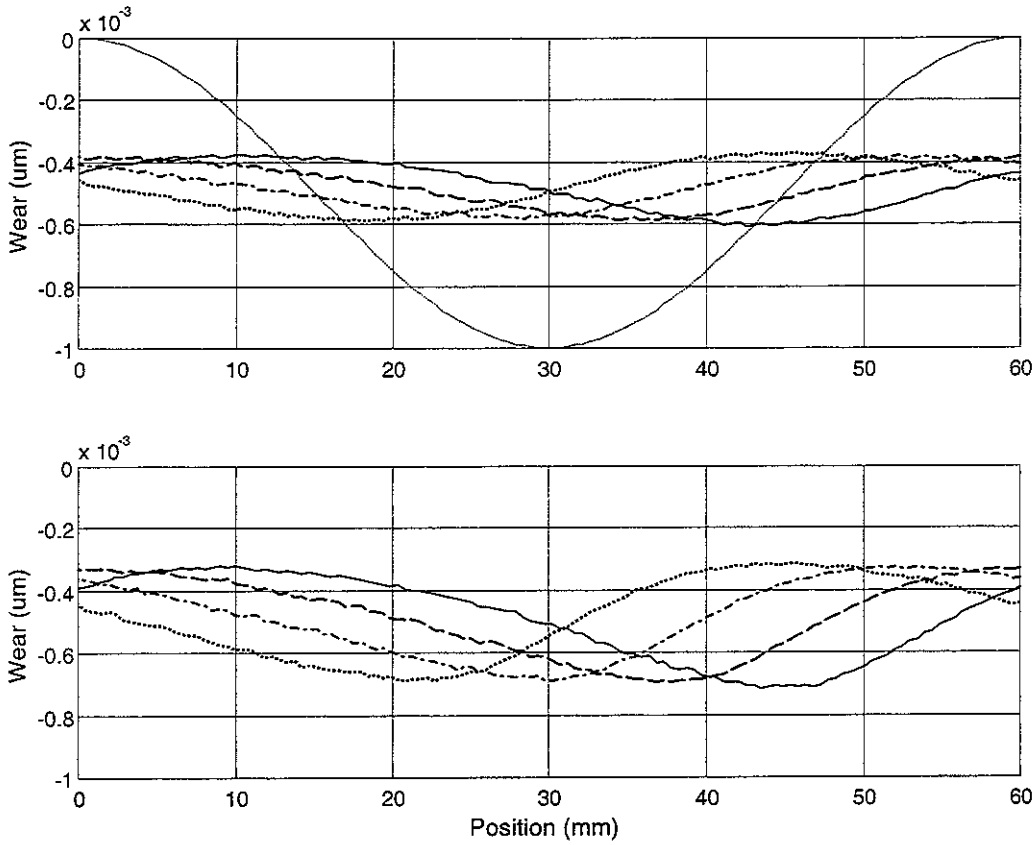


Figure 8. Wear due to micro-slip for corrugation wavelength $\lambda = 60$ mm, key as for Figure 6.

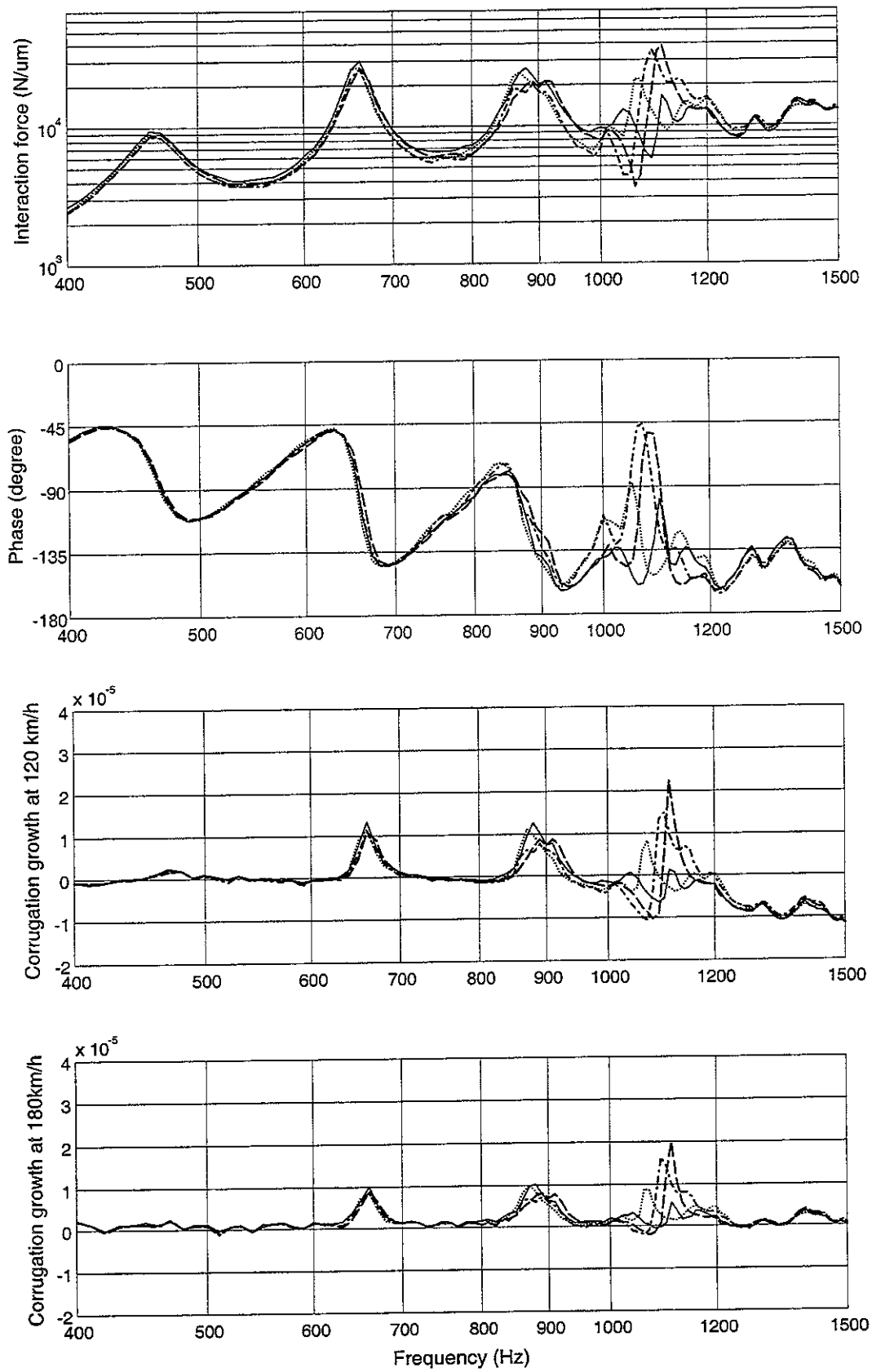


Figure 8. Corrugation growth rate after one passage of wheel 1 with soft rail pad. At 1 kHz wavelength $\lambda$ = 33, 50 mm for $V$ = 120, 180 km/h, respectively. — Wheel at sleeper, ---- at 1/4 span to the left of a sleeper, -·-·- at mid-span, ····· at 1/4 span to the right of a sleeper.

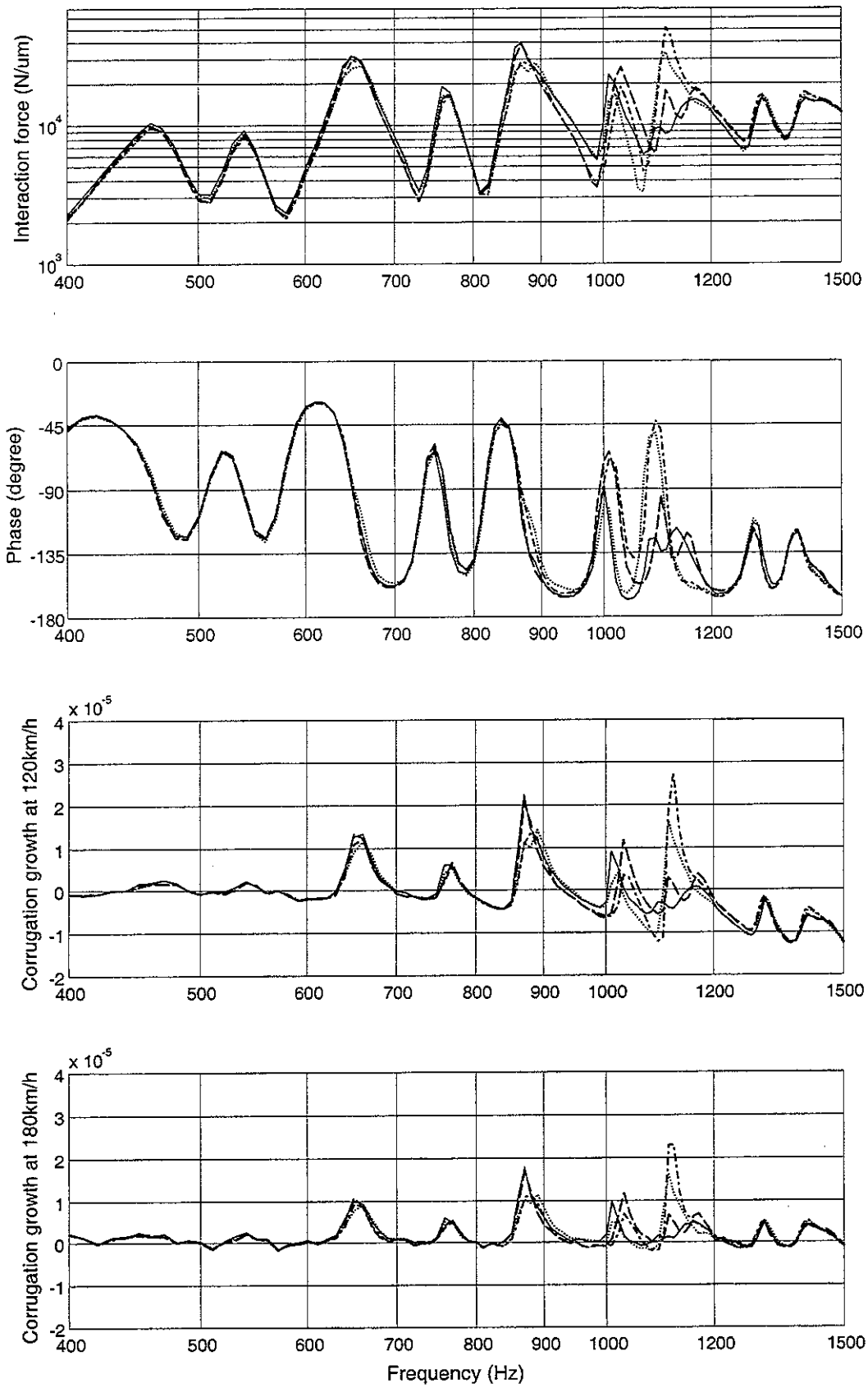


Figure 9. Corrugation growth rate after one passage of wheel 2 with soft rail pad, key as for Figure 8.

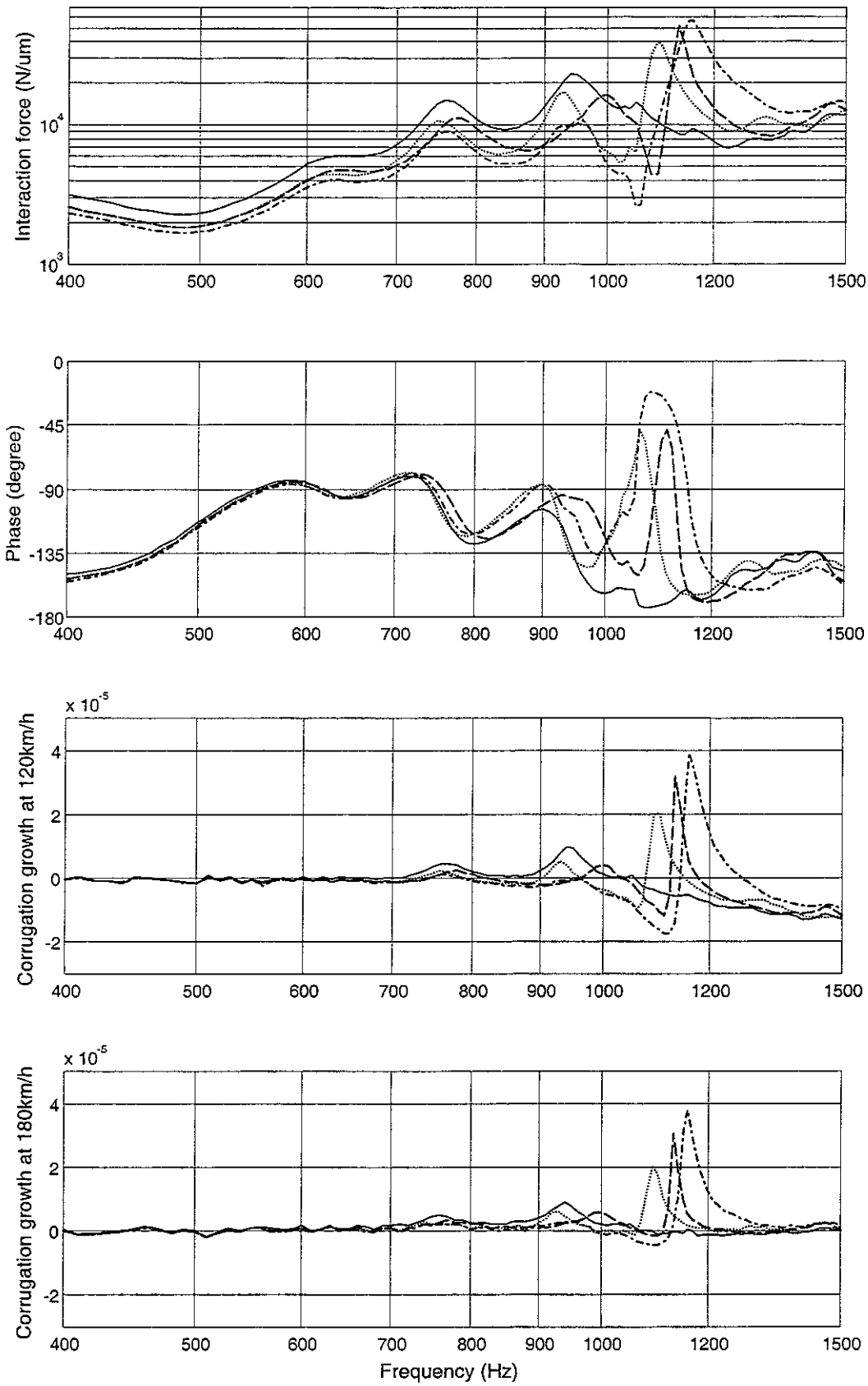


Figure 10. Corrugation growth rate after one passage of wheel 1 with medium rail pad, key as for Figure 8.

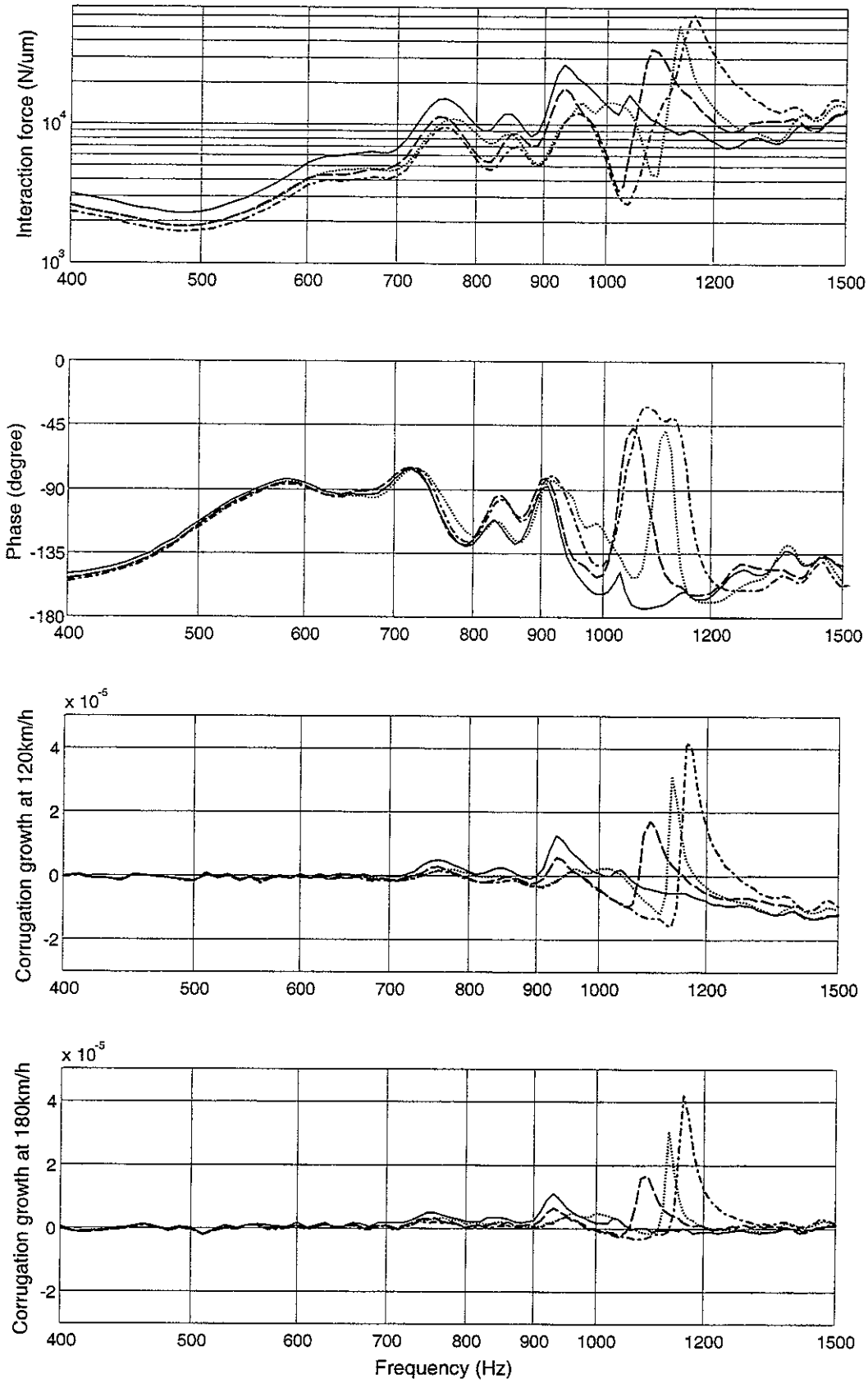


Figure 11. Corrugation growth rate after one passage of wheel 2 with medium rail pad, key as for Figure 8.

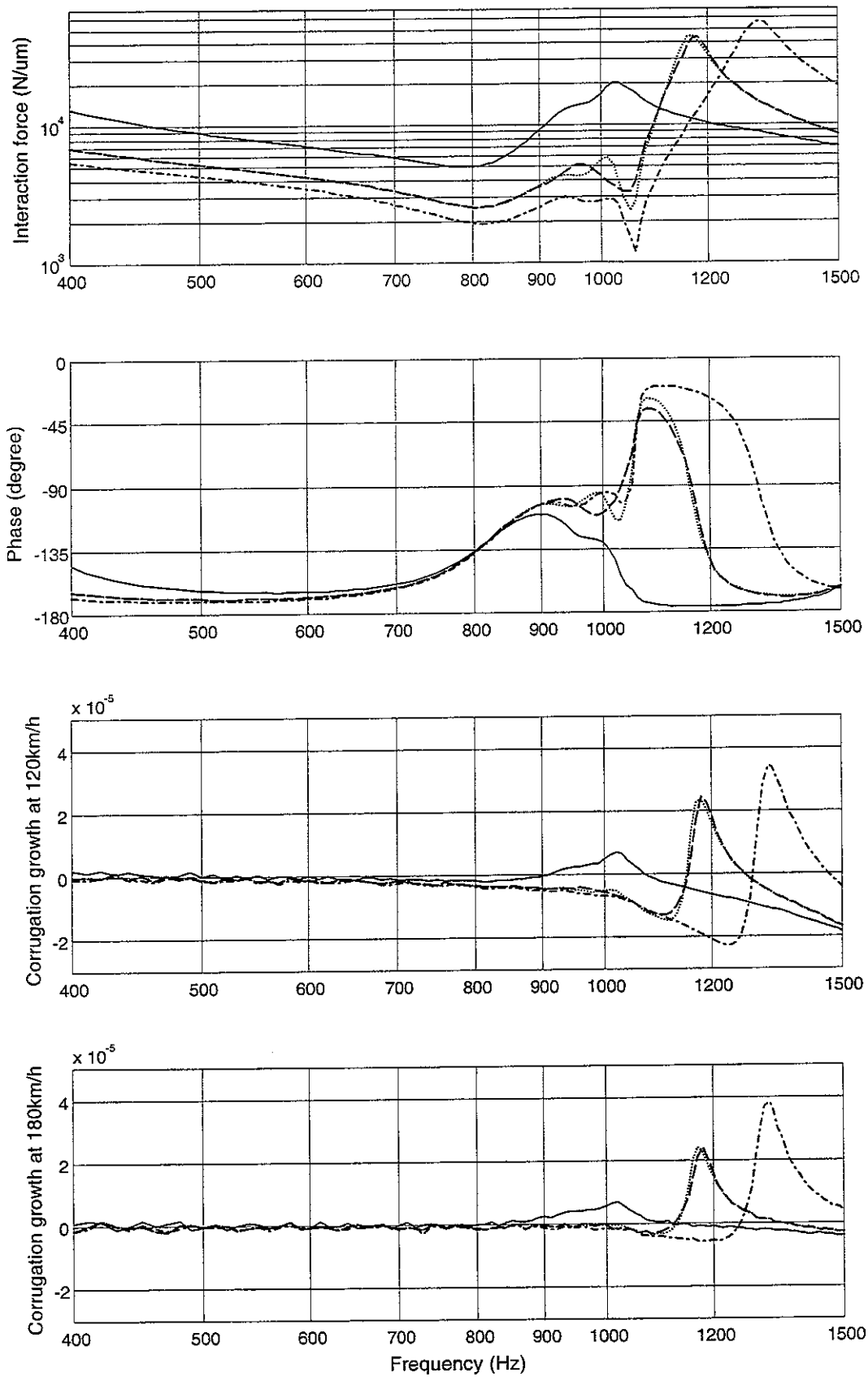


Figure 12. Corrugation growth rate after one passage of wheel 1 with stiff rail pad, key as for Figure 8.

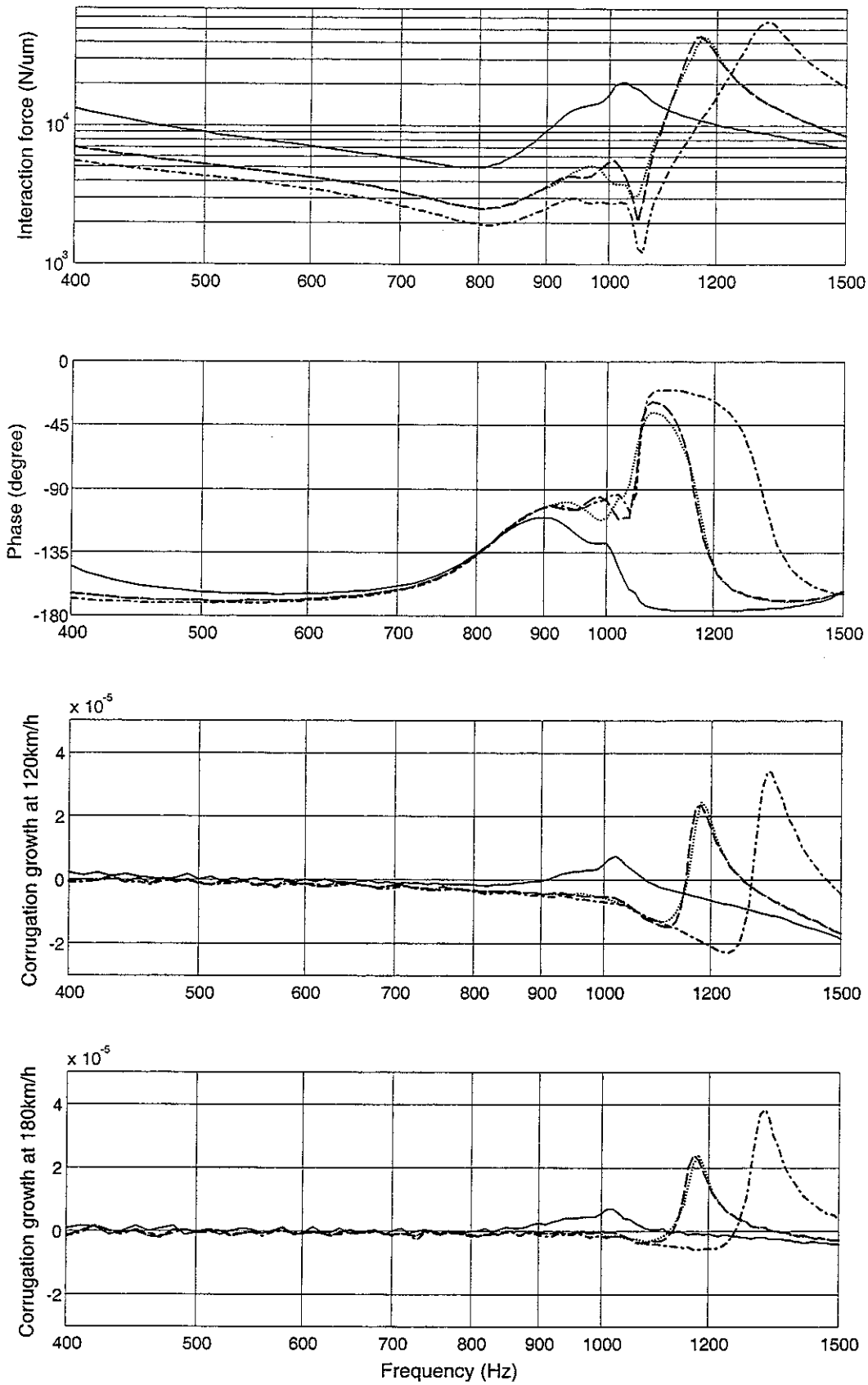


Figure 13. Corrugation growth rate after one passage of wheel 1 with stiff rail pad, key as for Figure 8.